land

MDPI

Article

Optimizing Urban Green–Gray Stormwater Infrastructure Through Resilience–Cost Trade-Off: An Application in Fengxi New City, China

Zhaowei Tang [1], Yanan Li [1], Mintong Hao [1], Sijun Huang [1], Xin Fu [1,*], Yuyang Mao [1] and Yujiao Zhang [2]

[1] College of Landscape Architecture & Arts, Northwest A&F University, Yangling 712100, China
[2] Institute of Surveying, Mapping and Geoinformation in Guangxi Zhuang Autonomous Region, Liuzhou 545006, China
* Correspondence: fuxinuc@outlook.com

Abstract

Accelerating urbanization and the intensifying pace of climate change have heightened the occurrence of urban pluvial flooding, threatening urban sustainability. As the preferred approach to urban stormwater management, coupled gray and green infrastructure (GI–GREI) integrates GREI's rapid runoff conveyance with GI's infiltration and storage capacities, and their siting and scale can affect life-cycle cost (LCC) and urban drainage system (UDS) resilience. Focusing on Fengxi New City, China, this study develops a multi-objective optimization framework for the GI–GREI system that integrates GI suitability and pipe-network importance assessments and evaluates the Pareto set through entropy-weighted TOPSIS. Across multiple rainfall return periods, the study explores optimal trade-offs between UDS resilience and LCC. Compared with the scenario where all suitable areas are implemented with GI (maximum), the TOPSIS-optimal schemes reduce total life-cycle cost (LCC) by CNY 3.762–4.298 billion (53.36% on average), rebalance cost shares between GI (42.8–47.2%) and GREI (52.8–57.2%), and enhance UDS resilience during periods of higher rainfall return (P = 20 and 50). This study provides an integrated optimization framework and practical guidance for designing cost-effective and resilient GI–GREI systems, supporting infrastructure investment decisions and climate-adaptive urban development.

Keywords: green–gray infrastructure; multi-objective optimization; life cycle cost; resilience

check for updates

Academic Editor: Zhonghua Gou

Received: 17 October 2025
Revised: 9 November 2025
Accepted: 9 November 2025
Published: 12 November 2025

Citation: Tang, Z.; Li, Y.; Hao, M.; Huang, S.; Fu, X.; Mao, Y.; Zhang, Y. Optimizing Urban Green–Gray Stormwater Infrastructure Through Resilience–Cost Trade-Off: An Application in Fengxi New City, China. *Land* **2025**, *14*, 2241. https://doi.org/10.3390/land14112241

Copyright: © 2025 by the authors. Licensee MDPI, Basel, Switzerland. This article is an open access article distributed under the terms and conditions of the Creative Commons Attribution (CC BY) license (https://creativecommons.org/licenses/by/4.0/).

1. Introduction

In recent years, global climate change has increased the frequency and intensity of extreme rainfall events [1,2], while rapid urbanization has substantially expanded impervious surfaces, thereby increasing surface runoff, disrupting the urban water cycle, and seriously threatening urban hydrologic safety [3–5]. Traditionally, stormwater management has relied on gray infrastructure (GREI), including pipes, channels, and culverts, to control surface runoff and mitigate flood risk. Although GREI can intercept, collect, and convey runoff for drainage, these conventional systems are increasingly viewed as inflexible and inefficient, leading to ecosystem degradation [6,7] and showing limited hydraulic performance under the pressures of urban development [8,9]. By contrast, green infrastructure (GI) effectively reduces surface runoff, enhances infiltration, and adapts to climate change [10–12]. GI also improves urban aesthetics and promotes sustainable urban development [13,14]. For example, rain gardens, permeable pavements, and green roofs have been widely promoted as small-scale solutions in dense urban areas [15]. Despite

these advantages, GI alone has limited effectiveness in managing runoff during extreme rainfall events and cannot entirely substitute for GREI [16,17].

Recent studies show that GI–GREI coupled planning can enhance drainage performance, reduce environmental impacts, lower costs, and strengthen system resilience [18–22]. A water security economic assessment framework further highlighted the potential of this coupling for improving urban hydrologic security and providing cost-effective infrastructure services [23]. A quantitative flooding adaptation model demonstrated that integrated GI–GREI strategies outperform conventional approaches in mitigating urban flood risk under extreme events [19]. Simulations of alternative GI–GREI configurations also indicated greater robustness compared to GREI-only schemes [24]. With these advances, scholars increasingly emphasize that proper GI–GREI configuration is critical to solving urban drainage challenges. Yet, scenario-based simulations alone are often inadequate for managing complex systems with multiple constraints. Consequently, recent research has turned to multi-objective optimization frameworks to identify optimal GI–GREI coupling strategies [21,25,26].

The optimal coupling of GI and GREI must account for technical, economic, and ecological constraints while balancing trade-offs between functions and benefits [27–29]. Traditional optimization methods, such as enumeration and linear programming, often struggle to address this complexity and diversity of constraints [30]. Recent studies show that integrating urban hydrologic models with multi-objective optimization algorithms has substantially advanced GI–GREI coupling configurations [22,31,32]. Metaheuristic methods are widely applied due to their strong ability to solve nonlinear and discrete problems [33], including genetic algorithms (GAs), ant colony optimization, simulated annealing, and particle swarm optimization [34]. Among these, NSGA-II is highly regarded for its solution diversity and convergence performance. The optimization framework needs support from hydrologic modeling to assess its runoff control performance. The mainstream tools include InfoWorks ICM, MIKE+, SUSTAIN, and SWMM, each offering distinct characteristics and applications [35]. Owing to its open-source nature, SWMM can be flexibly integrated with programming languages and multi-objective optimization algorithms. Its robust hydrologic and hydraulic simulation capabilities also make it one of the most frequently used tools in optimization studies.

In recent studies, SWMM has been combined with NSGA-II to optimize the siting and sizing of GI. The results effectively identified optimal locations and scales, although the focus on a single GI type overlooked the synergistic advantages of composite strategies [15]. A two-objective NSGA-II model, targeting pollutant reduction and fiscal efficiency, optimized the siting of GREI and GI separately, providing the optimal layouts for permeable pavement, green roofs, and rain barrels in the study area [36]. From a life-cycle perspective, optimization has emphasized the sustainability of GREI and GI. Under climate change conditions, multi-objective optimization of coupled GI–GREI configurations has identified sustainable strategies capable of withstanding climate-related impacts [21]. Some studies have further integrated urban resilience metrics into optimization frameworks, deriving GI–GREI configurations aligned with resilience objectives by refining deployment strategies and portfolio compositions [37]. In addition, constraints such as storm sewer design standards have been embedded into the optimization to ensure engineering feasibility. By adjusting drainage pipe diameters and GI placement, studies have developed practical implementation strategies that improve applicability under real-world conditions [8]. Collectively, these studies highlight that under multiple objectives and constraints, hydrologic, environmental, and resilience-based optimization of GI and GREI not only enhances urban water security but also provides effective frameworks to address complex urban drainage challenges [38–40].

However, existing studies rarely incorporate the hierarchy and corresponding sizing of drainage pipe networks or the coordination and connectivity of GI–GREI into the optimization process to address cost-optimal stormwater facility configuration under sewershed or watershed resilience. In addition, many studies focus only on generating the Pareto optimal set without performing further evaluation or prioritization to identify solutions suitable for practical implementation. To address these shortcomings, this study proposes using an NSGA-II and SWMM model to develop a multi-objective optimization framework that integrates GI and GREI under multiple rainfall scenarios. The framework trades off UDS resilience against LCC to evaluate the effectiveness of combining GI and GREI in terms of both quantity and spatial distribution. The existing pipe network is divided into three tiers and optimized separately under engineering feasibility constraints to enhance implementation.

This study advances GI–GREI optimization by integrating their attributes, spatial distributions, and hierarchical structures, thereby providing a framework to enhance urban flood resilience. It offers evidence-based insights to guide the planning and design, construction sequencing, and investment allocation of stormwater infrastructure. Furthermore, it establishes a coherent framework for assessing and optimizing hybrid stormwater systems, supporting both future research and practical applications in resilient urban infrastructure planning. The results offer practical insights for planners and policymakers to develop cost-efficient and resilient stormwater solutions within engineering and financial constraints, supporting sustainable, low-carbon, and climate-adaptive urban development.

2. Materials and Methods

2.1. Research Framework

The workflow consists of three stages (Figure 1). First, we developed an SWMM model to represent three types of GI together with the pipe network. Second, we constructed an NSGA-II model in PyGMO (v2.19.7), using LCC and UDS resilience as objectives, with decision variables including GI quantity and layout as well as pipe diameter. Third, optimization was conducted within the NSGA-II framework integrating PySWMM (v2.1.0) in Python (v3.12.11) scripts to generate Pareto sets. Finally, the entropy-weighted TOPSIS method was applied to rank the solutions and identify the optimal scheme to guide implementation.

2.2. Study Area and Data Collection

Fengxi New City, one of the five clusters of the Xixian New Area, is located at the interface between Xi'an's westward expansion and Xianyang's eastward extension and is planned as the core carrier of Xi'an–Xianyang integration, linking the two cities through industrial and transportation integration (https://en.shaanxi.gov.cn/business/dz/ndz/201709/t20170907_1594661.html accessed on 15 November 2024; Figure 2). The study area covers 143 km^2. By the end of 2021, Fengxi New City had a resident population of approximately 0.30 million and a GDP of around CNY 13.4 billion. The area has a mean annual precipitation of approximately 650–700 mm. Rainfall is highly concentrated in summer, often resulting in short-duration peak runoff. In 2015, Fengxi New City was approved as one of the national Sponge City pilot sites, an urban water management approach that enhances on-site infiltration, retention, purification, and controlled release of stormwater to mitigate flooding and improve reuse, where GI practices and trial stormwater management facilities have been systematically implemented. Most of the data employed in this study were obtained from public or governmental datasets (Table 1). The land use is digitalized and interpretated based on satellite images from CF-6 with an 8 m spatial resolution. The current pipelines' directions, depths, and diameters provided in the Special

Plan for Stormwater Engineering in Fengxi New City are used to derive the network topology and assemble the pipe network for the study area.

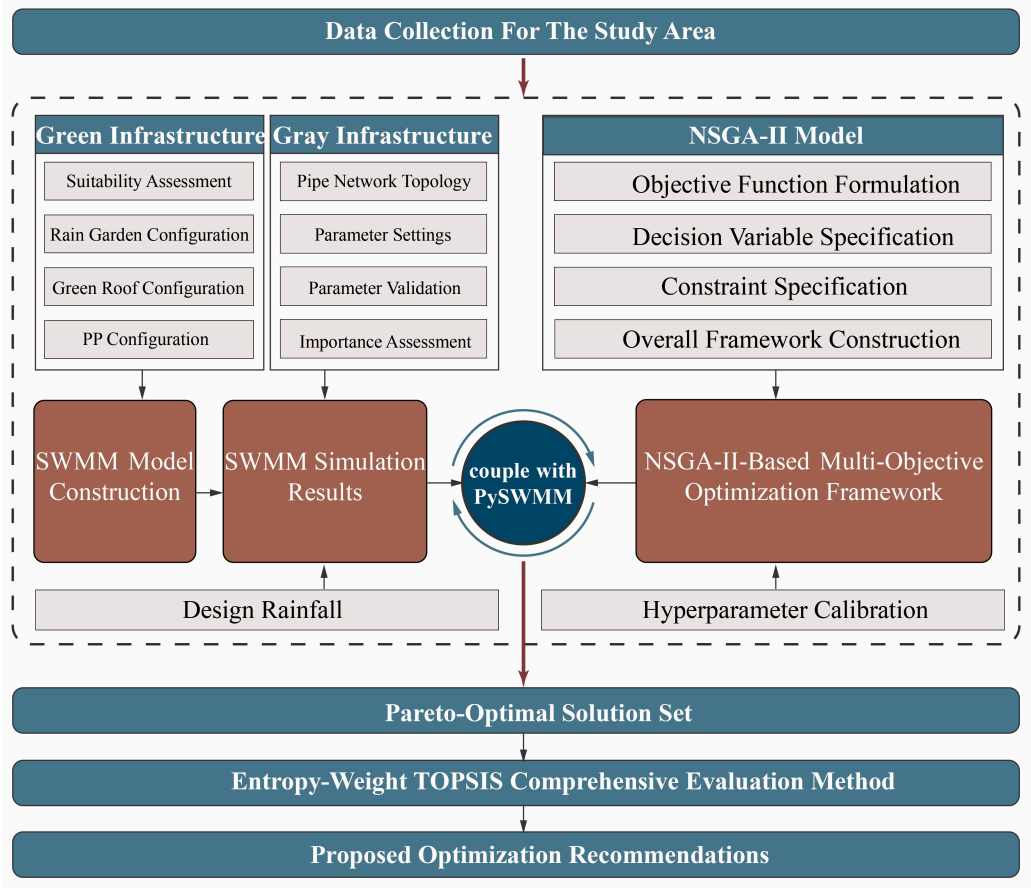


Figure 1. Research design and dataflow.

Table 1. Data sources.

Data	Type	Source	Access Date
Satellite Image	Raster	https://www.gscloud.cn/, accessed on 14 July 2024	June 2024
DEM	Raster	https://www.gscloud.cn/, accessed on 10 April 2025	April 2025
Building footprint	Vector	https://lbsyun.baidu.com/, accessed on 10 April 2025	April 2025
Sidewalks	Vector	https://lbsyun.baidu.com/, accessed on 11 April 2025	April 2025
Park boundary	Vector	https://lbsyun.baidu.com/, accessed on 11 April 2025	April 2025
Pipelines	Vector	Special Plan for Stormwater Engineering in Fengxi New City	April 2024
Construction prices for GREI	Table	https://www.zjtcn.com/, accessed on 1 May 2025	May 2025
Construction prices for GI	Table	https://www.zjtcn.com/, accessed on 1 May 2025	May 2025

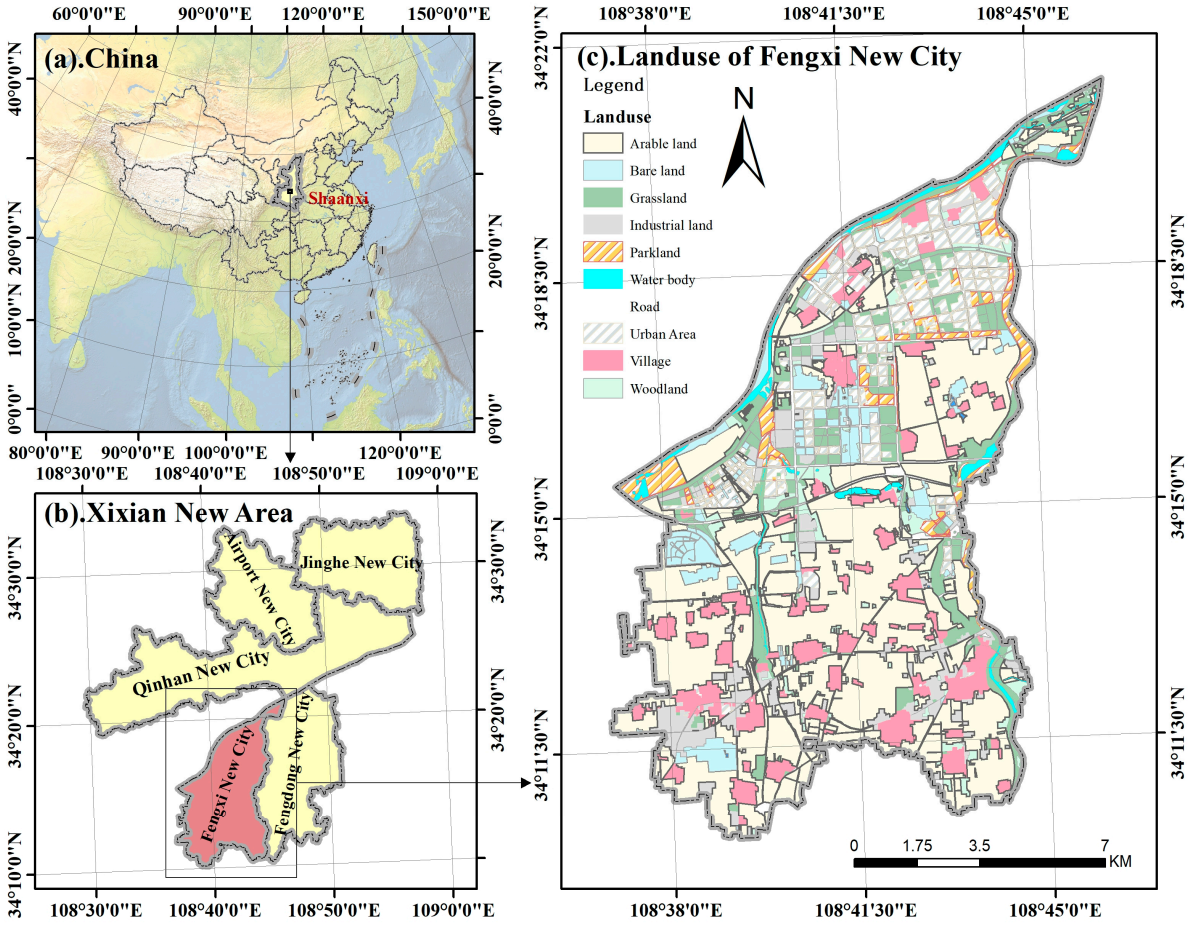


Figure 2. Study area locations and land use.

2.3. Suitability Analysis of GI

Three types of green infrastructure (GI), including green roofs (GRs), rain gardens (RGs), and permeable pavements (PPs), are considered for their demonstrated effectiveness in mitigating runoff and their relative cost-effectiveness [41]. Rain barrels were not included because they are primarily applicable to low-rise buildings, whereas most buildings in Fengxi New City are multi-story or high-rise structures. For GR, suitability is primarily determined by roof characteristics and structural load capacity, including service life and construction materials. In contrast, the suitability of RGs and PPs is mainly influenced by slope, soil conditions, and proximity to buildings. The domains and scoring rules for the three GI types follow Mao et al., 2024 [24]. In the suitability evaluation of green roofs, both roof type (flat or pitched) and load-bearing capacity were considered. The latter was represented by the building's design service life and structural form. Buildings with a design service life of 50 years or constructed with reinforced concrete were regarded as capable of supporting additional loads. The Analytic Hierarchy Process (AHP) is applied to weight the GI suitability criteria. A three-level hierarchy is constructed, and experts perform pairwise comparisons using the Saaty 1–9 scale, where a consistency ratio (CR) ≤ 0.10 is accepted. The resulting weights are then combined with the criteria scores and normalized to a 0–1 scale, yielding a composite suitability index for optimization.

2.4. SWMM Model Configuration

Based on the Special Plan for Stormwater Engineering of Fengxi New City, Shaanxi, together with DEM and imagery, we delineated the urban drainage pipelines for the study area. The final model divides the area into 878 sub-catchments and represents the drainage

network, which has 878 conduit segments, 878 junctions (manholes), and 23 outfalls. The total drainage area is 9098.61 ha.

2.4.1. Design Storms

Based on the Low-Impact Development Technical Guide for Sponge City Construction (Trial) of the Xixian New Area, the parameters of the regional intensity–duration–frequency (IDF) relationship are obtained for the study area, as expressed in Equation (1). The Chicago hyetograph was applied to distribute rainfall, using a storm duration of 60 min, a peak position coefficient of 0.405, and a time step of 1 min. Storm events with return periods of 2, 5, 10, 20, and 50 years were simulated (Figure 3).

$$q = \frac{2785.833(1 + 1.658lgP)}{(t + 16.813)^{0.9302}} \quad (1)$$

where q is design rainfall intensity [L/(s·ha)]; P is design return period (years); and t is storm duration (min).

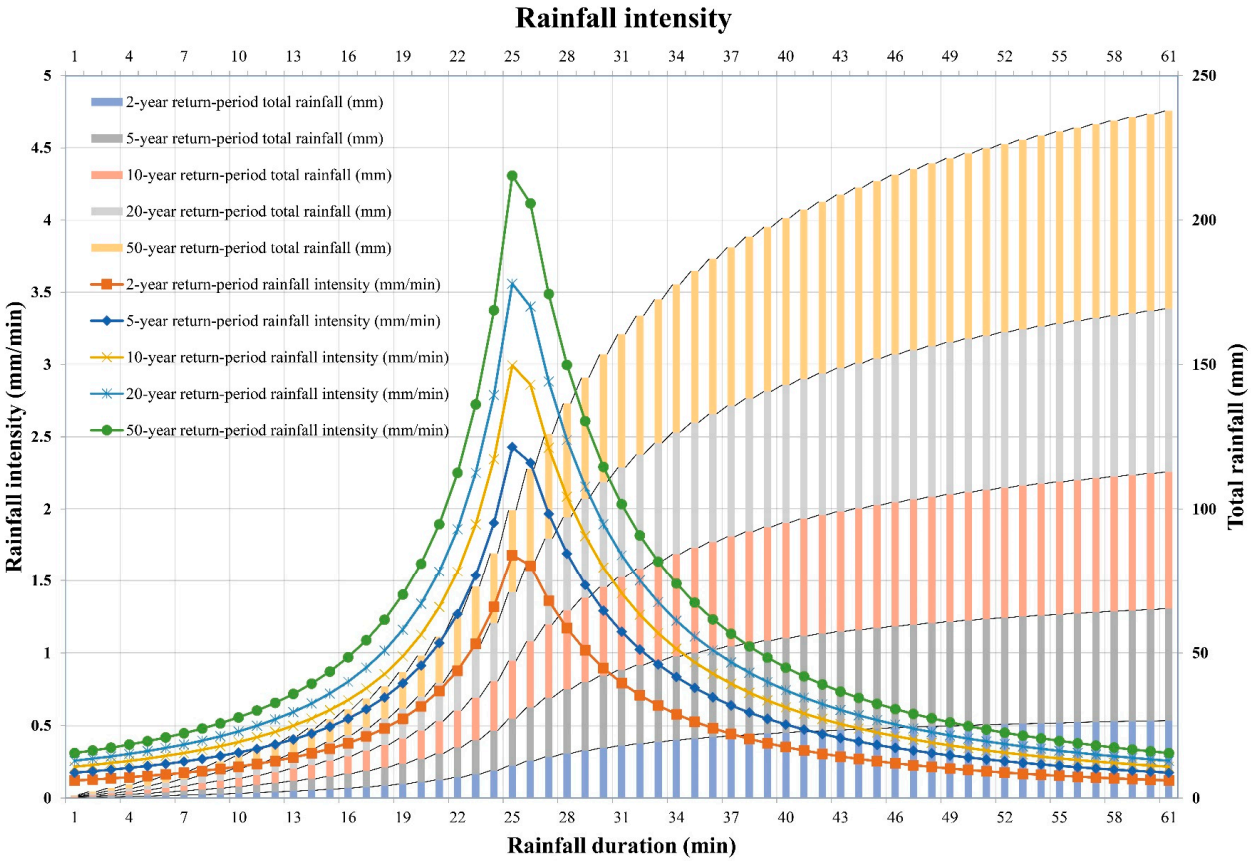


Figure 3. Rainfall distributions for different return periods.

2.4.2. SWMM Model Calibration and Parameter Determination

According to the land-use data analysis, the study area has an overall imperviousness of 34.8%. Meanwhile, it contains extensive woodland, green spaces, and cultivated land. Mean sub-catchment slopes were obtained from the DEM. In constructing the SWMM model, catchment width and slope are physical parameters defining the geometric characteristics of each sub-catchment. Each sub-catchment's width and slope were specified individually from the digital elevation model (DEM) and land-use data. Infiltration losses and pipe-flow routing were represented using the Horton method and the kinematic wave approach, respectively. Initial parameters for sub-catchments and GI were obtained based

on the SWMM Reference Manual, watershed characteristics, and relevant literature, and were further refined during calibration.

Due to limited runoff and outfall monitoring data in the study area, the comprehensive runoff coefficient method was adopted for SWMM validation. Model parameters were adjusted by comparing simulated runoff coefficients with empirical values. A sensitivity analysis was conducted for each calibration parameter using Spearman's rank correlation to quantify their influence on runoff. Depression storage on pervious areas and Manning's roughness for impervious areas, which exhibited correlation coefficients greater than 0.5, were identified as the most sensitive parameters. In Fengxi New City, the municipal drainage system is designed for a 2-year return period in most areas and for a 3-year return period in areas of higher importance. Using this method, the model runoff coefficient was estimated to range between 0.41 and 0.46. According to the Code for Design of Outdoor Wastewater Engineering (GB 50014-2021), empirical runoff coefficients for land cover with 30 to 50 percent imperviousness typically range from 0.4 to 0.6. This comparison verifies the robustness of the SWMM model, as well as the suitability of the chosen parameters. The calibrated parameters are summarized in Table 2.

Table 2. Parameters of SWMM after calibration.

Category	Item	Parameter
Sub-catchment and Network Parameters	Manning's n for impervious areas	0.013
	Manning's *n* for pervious areas	0.25
	Depression storage on impervious areas (mm)	2.1
	Depression storage on pervious areas (mm)	3.6
	Percentage of impervious area with zero depression storage (%)	25
	Horton maximum infiltration rate (mm/h)	25.67
	Horton minimum infiltration rate (mm/h)	3.43
	Horton decay constant (1/h)	7
	Drying time from saturation to fully dry (days)	7
	Manning's *n* for conduits	0.013

2.5. Drainage Pipe Network Importance Assessment

This study introduces the concept of pipe network importance to guide the selection of parameter ranges, step sizes, and update sequences for pipelines in the optimization process, based on flow convergence direction and network topology. By identifying and ranking critical components within the system, we quantify each conduit's criticality using the indicator I_i, where I_i denotes the importance of pipe i, as defined by Equation (2).

$$I_i = \frac{C_{max} - C_i}{C_{max} - C_{min}} = \frac{C_{max} - \left(1 - \frac{A_i}{A_t}\right)}{C_{max} - C_{min}} \quad (2)$$

where A_i represents areas of sub-catchments upstream flowing into pipe i; A_t is the total area of all sub-catchments; $C_i = \left(1 - \frac{A_i}{A_t}\right)$ is the raw network coefficient, with smaller values indicating a more critical pipe; C_{max}, C_{min} are the maximum and minimum C_i across all pipes, respectively; and I_i is the normalized pipe-importance index in $[0, 1]$, with larger values indicating higher criticality.

By calculating and ranking I_i, we facilitate the subsequent optimization by assigning greater weight to critical conduits, thereby prioritizing investments that enhance system-wide retrofit benefits. This approach also allows computational effort to be allocated more efficiently, reducing the time spent on segments with limited potential for improvement and improving both the rigor and efficiency of the optimization process.

2.6. GI–GREI Optimization via the NSGA-II Algorithm

2.6.1. Development of the NSGA-II Model

NSGA-II, incorporating fast non-dominated sorting, crowding-distance preservation, and an elitist strategy, ensures efficient convergence and high-quality iterations. We implemented NSGA-II in Python using the PyGMO framework, applying core operators including crossover, mutation, non-dominated sorting, crowding-distance assignment, and binary tournament selection. Modular code was developed to integrate objective functions, decision variables, and constraints into the algorithm. The results were post-processed with NumPy (v2.4.3) and visualized using Matplotlib (v3.10.7).

Multi-objective optimization aims to identify a set of solutions that achieve Pareto-optimal trade-offs among conflicting criteria under given constraints. In this study, the mathematical formulation for GI–GREI optimization is presented in Equation (3).

$$d_{\text{opt}} = \underset{d \in D}{\text{argmax}}[\langle f_{-LCC} \rangle, \langle f_{\text{UDS}-R} \rangle] \tag{3}$$

where d_{opt} is the optimal configuration of the GI–GREI decision vector d; f_{-LCC} is the objective to be maximized that corresponds to minimizing life-cycle cost; and $f_{\text{UDS}-R}$ is the objective to be maximized that corresponds to maximizing UDS resilience.

2.6.2. Objective Functions

(1) Life-Cycle Cost (LCC)

Life-cycle cost (LCC) represents the total direct and indirect expenditures of an asset over its entire life, including planning, design, construction, operation, maintenance, and end-of-life disposal. For the GI and GREI systems, LCC comprises construction (capital) costs and the present value of operation and maintenance (O&M) costs. The equations for the LCC and O&M present value are given in Equations (4)–(6). The construction–cost data are sourced from the local building-materials market, and the details are provided by the Equation (7) and Table 3. Annual O&M costs for GI and GREI are assumed to be 8% and 10% of their respective construction costs [15].

$$\text{LCC} = \text{Capital}_{\text{GREI}} + \text{Capital}_{\text{GI}} + \text{PV}_{\text{O\&M GREI}} + \text{PV}_{\text{O\&M GI}} \tag{4}$$

$$\text{PV}_{\text{O \&M}_{\text{GREI}}} = \sum_{1}^{\text{n}} \text{O \&M}_{\text{GREI}} \frac{1}{(1+\text{i})^{\text{n}}} \tag{5}$$

$$PV_{O\&M_{GI}} = \sum_{1}^{n} \text{O\&M}_{\text{GI}} \frac{1}{(1+\text{i})^{n}} \tag{6}$$

where $Capital_{GREI}$ is the construction (capital) cost of GREI; $Capital_{GI}$ is the construction (capital) cost of GI; $PV_{O\&M,GREI}$ is the present value of O&M costs for GREI; $PV_{O\&M,GI}$ is the present value of O&M costs for GI; i is the local annual discount rate (set to 2%); and n is the life-cycle length (set to 30 years).

Table 3. Cost for different types of GI (based on local market average price).

GI	Rain Garden	Permeable Pavement	Green Roof
Construction cost (CNY/m^2)	150–1200	60–350	100–500
Maintenance cost (CNY/m^2/year)	12–96	5–28	8–40

For GREI, the unit pipe construction cost model proposed by Houle et al. [42] was adopted, as shown in Equation (7).

$$C = K_1 + K_2H + K_3H^2 + K_4DH + K_5D + K_6D^2 + K_7D^3 \quad (7)$$

where C is the unit pipe cost (CNY per 100 m); D is the pipe diameter (m); H is the burial depth (m); and $K_1, K_2, \ldots, K_7$ are the locale-specific coefficients. Using a pipe network cost linear regression model to identify local $K_1, K_2, \ldots, K_7$ [43], the model was fitted (R^2 = 0.7784; in SPSS IBM, version 27.0) using construction data for pipeline construction projects in the Central China market for May 2025. The resulting coefficients are $K_1 = -207.575$, $K_2 = -284.496$, $K_3 = -494.939$, $K_4 = 2449.130$, $K_5 = 1223.499$, $K_6 = -802.996$, $K_7 = 63.141$.

(2) Urban Drainage System Resilience

UDS resilience is introduced as the second objective in the optimization. It is quantified based on the severity and duration of functional failures during rainfall events (e.g., surcharge, overflow) [44]. The estimation method is provided in Equation (8).

$$R_f = 1 - \frac{V_{TF}}{V_{TI}} \times \frac{t_f}{t_n} \quad (8)$$

where R_f is the determined by measuring the residual functionality of the system; V_{TF} is the total flood volume at all inundated nodes; V_{TI} is the total inflow volume to the system; t_f is the average inundation duration across all flooded nodes; t_n is the total simulation time; and $R_f \in [0, 1]$.

2.6.3. Decision Variables

Decision variables define the feasible solution space and link the objective functions to the constraints, which specify the physical, technical, or managerial requirements the variables must satisfy [45,46].

Based on the GI suitability analysis, the upper bound of each GI type's area is set as the maximum value for its corresponding decision variable. In each NSGA-II iteration, constrained stochastic perturbations are applied to the allocated areas of the three GI types. This approach expands the solution space, improves search coverage, and allows the identification of a greater number of engineering-feasible configurations.

The municipal drainage network exhibits a clear hierarchy, with higher-tier pipes conveying larger confluences and therefore requiring larger diameters. Pipe diameters are also constrained by design codes and must be selected from a limited range of discrete sizes. To enhance computational efficiency, we first perform a pipe-importance analysis and then classify existing diameters using the natural breaks (Jenks) method into three tiers: trunk pipes, secondary pipes, and branch pipes. For each tier, a realistic, bounded range of admissible diameters is specified (Table 4).

Table 4. Diameter ranges for three-level pipe network.

	Trunk Sewers	**Secondary Sewers**	**Branch Sewers**
Diameter range (m)	1.5–2.8	0.8–2.2	0.5–1.5

2.6.4. Constraints

Constraints define the feasible solution space by incorporating engineering limits and decision rules, such as resource caps, physical bounds, and regulatory requirements. Engineering feasibility is maintained through penalty terms and a repair operator, ensuring that solutions violating constraints are penalized or corrected before selection, crossover, and mutation. This guides the evolutionary search toward the feasible region and accelerates identification of the Pareto front.

For example, GI can only be installed within candidate zones identified by the suitability evaluation. For each sub-catchment and GI type, the buildable area ranges from zero to the maximum suitable area. The diameters of pipes must lie between 0.5 and 2.8 m and be chosen from commercially available discrete sizes. Its step changes follow the C-value requirement of the cost model shown as Equation (9), reflecting the unit-cost discretization. For the hydraulic constraint, along any flow path, upstream diameters should not exceed downstream diameters.

$$0 \leq d_{i+1} - d_i = C \tag{9}$$

where d_i is the upstream pipe diameter; d_{i+1} is the downstream pipe diameter; and C is measured in millimeters (mm) (a constant that is an integer multiple of 100).

2.6.5. Formulation of the Multi-Objective Optimization Model

The core NSGA-II modules include binary tournament selection, simulated binary crossover (SBX), polynomial mutation with a distribution index, fast non-dominated sorting, and crowding-distance computation. For this study, parameters were based on recent NSGA-II optimization studies [47,48] and further calibrated through preliminary experiments to achieve a configuration that balances convergence and search breadth (Table 5).

Table 5. Parameter settings for running NSGA-II.

Parameter	Description	Setting
Population size	Number of individuals per generation	600
Tournament size	Tournament size for parent selection	2
Crossover probability	Probability that genetic crossover occurs	0.8
Crossover distribution index	SBX distribution index controlling offspring proximity to parents	5
Mutation probability	Probability that mutation occurs	0.25
Mutation distribution index	Polynomial-mutation distribution index controlling mutation magnitude	8
Number of generations	Maximum number of algorithm iterations	100

2.7. Entropy-Weighted TOPSIS Comprehensive Evaluation

After obtaining the Pareto set, TOPSIS (Technique for Order Preference by Similarity to Ideal Solution) is employed to find the optimal alternative by using the objective functions as evaluation indicators and entropy weighting. In the entropy weighting process, indicators with greater dispersion receive higher weights, emphasizing those with stronger discriminative power [24,45]. For each rainfall return period, UDS resilience (benefit-type) and LCC (cost-type) are weighted and incorporated into the TOPSIS ranking. The weighting procedure and equations are described in Wang et al. [48].

Let $i = 1, \ldots, M$ index the candidate schemes (Pareto solutions) under a given return period T, and $j = 1, \ldots, J$ index the indicators (here $J = 2$: UDS resilience as benefit-type; LCC as cost-type). Denote via $y_{ij}^{(T)} \in [0, 1]$ the direction-consistent, min–max–normalized

matrix from the preceding EWM step (benefit indicators scaled higher is better, cost indicators reversed). Let $w_j^{(T)}$ be the entropy weights.

(1) Weighted normalized decision matrix

$$z_{ij}^{(T)} = w_j^{(T)} y_{ij}^{(T)} \quad (i = 1, \ldots, M; j = 1, \ldots, J). \tag{10}$$

(2) Positive/negative ideal solutions

Since $y_{ij}^{(T)}$ has been oriented so that larger is better,

$$\begin{aligned} z_j^{(T)+} &= \max_i z_{ij}^{(T)}, \\ z_j^{(T)-} &= \min_i z_{ij}^{(T)} \\ (j &= 1, \ldots, J). \end{aligned} \tag{11}$$

(3) Separation measures (Euclidean distance)

$$\begin{aligned} S_i^{(T)+} &= \sqrt{\sum_{j=1}^{J} \left(z_{ij}^{(T)} - z_j^{(T)+}\right)^2} \\ S_i^{(T)-} &= \sqrt{\sum_{j=1}^{J} \left(z_{ij}^{(T)} - z_j^{(T)-}\right)^2} \end{aligned} \tag{12}$$

(4) Closeness coefficient and ranking

$$C_i^{(T)} = \frac{S_i^{(T)-}}{S_i^{(T)+} + S_i^{(T)-}} \in [0, 1] \tag{13}$$

where a larger $C_i^{(T)}$ indicates a scheme closer to the PIS and farther from the NIS. Rank the schemes in descending order of $C_i^{(T)}$ to obtain the TOPSIS preference ordering for return period T.

3. Results

3.1. GI Suitability Evaluation Results

Five planning and engineering experts scored the suitability factors for each GI. Using the analytic hierarchy process (AHP), indicator weights were derived within each GI category. Consistency ratios (CRs) for green roofs, rain gardens, and permeable pavements were below 0.10, indicating reliable weights (Table 6). The weighted combination in ArcGIS (v10.8.1) was employed to compute suitability scores for each type of GI. The suitability areas for green roofs, rain gardens, and permeable pavements were 336.92 ha, 1294.15 ha, and 177.39 ha, respectively. The GI identified through this suitability evaluation is shown in Figure 4. It is evident that the different types of GI are predominantly concentrated in the northwestern part of the site, with relatively sparse distribution in the southern area. These identified areas were subsequently imported into the SWMM LIDs control module for further analysis.

Table 6. Weights of GI suitability evaluation indicators.

GI Type	Criterion	Weight
Green roof	Roof type	0.7231
	Building service life	0.1364
	Structural system	0.1405
Rain garden	Slope	0.1832
	Soil type	0.7081
	Distance from buildings	0.1087
Permeable pavement	Slope	0.1137
	Soil type	0.6654
	Distance from buildings	0.2209

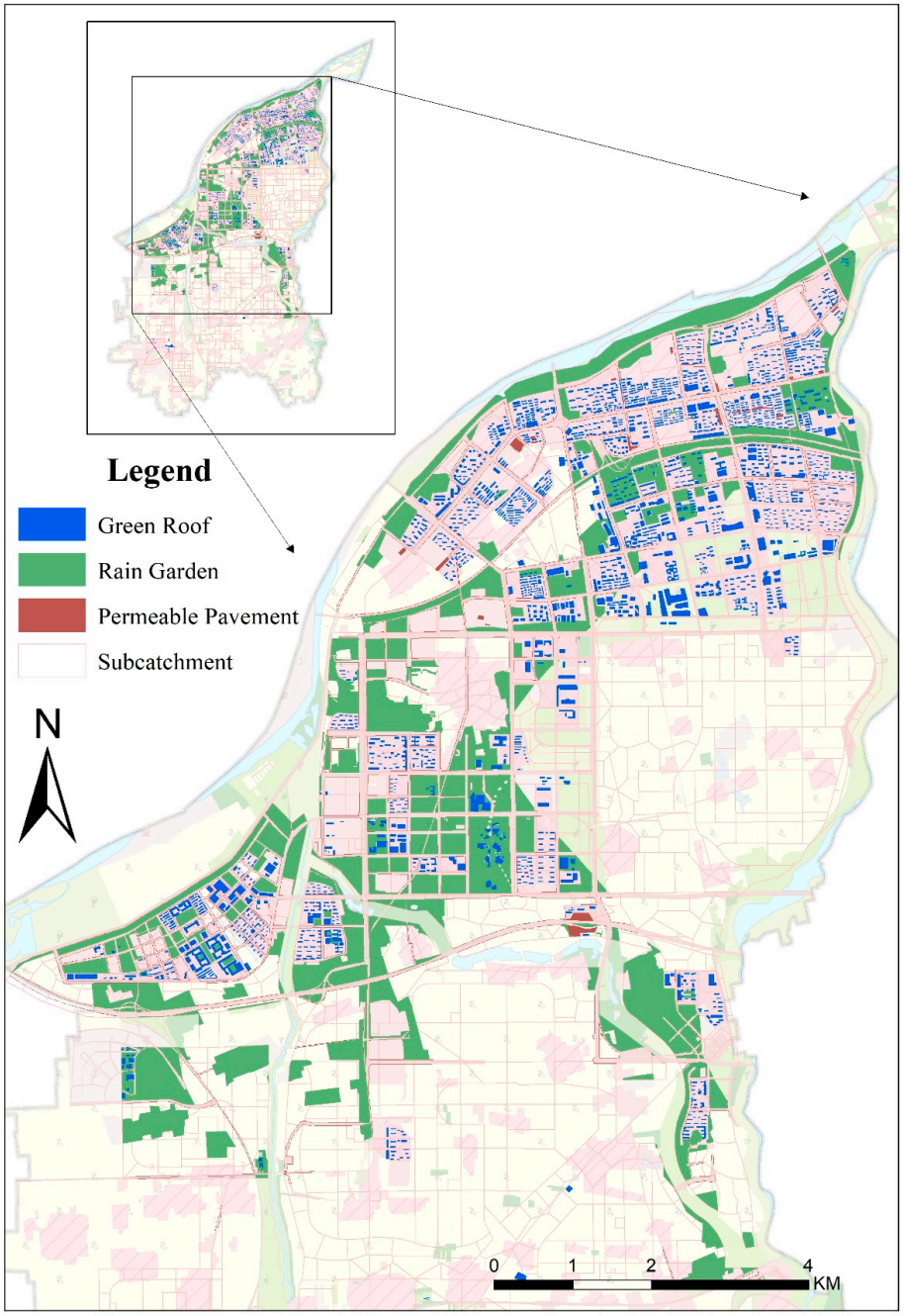


Figure 4. GI suitability evaluation results.

3.2. Pipe Network Importance Evaluation

The 878 conduit segments in the urban drainage network were classified into trunk, secondary, and branch types. The pipe-importance index I_i has a mean of 0.1310, a median of 0.0422, a standard deviation of 0.1969, and quartiles Q1 = 0.0145 and Q3 = 0.1494 (Table 7). Using natural-break thresholds of 0.1718 and 0.4979, 61, 132, and 685 segments were classified as high, medium, and low importance, representing 6.95%, 15.04%, and 78.01% of the total network length. High-importance pipe segments are concentrated along major drainage corridors and downstream areas near outfalls, while medium-importance segments appear along connector lines and low-importance segments are primarily found on peripheral or lateral branches. Network-based spatial autocorrelation analysis yields Moran's I = 0.8083 (P = 0.042 < 0.05), indicating significant spatial clustering of the importance index.

Table 7. Examples for critical pipe segments.

Pipe ID	Upstream Contributing Area (ha)	Importance Index	Rank
C00411	1193.492	1.0000	1
C00410	584.517	0.4979	61
C00426	205.574	0.1718	193

3.3. Multi-Objective Optimization Results

Figure 5 presents the global solution space and Pareto fronts for five return periods (P = 2, 5, 10, 20, and 50 years). In each scenario, solutions gradually converge toward the non-dominated region characterized by lower LCC and higher UDS resilience, with intergenerational improvements diminishing over iterations. Aggregated across scenarios, the final Pareto sets covered LCC values from CNY 2.17 to 7.12 billion and UDS resilience from 0.545 to 0.983. The Pareto solutions distributed evenly across the objective space, with similar front morphology observed among scenarios. The upper and lower bounds of UDS resilience decreased as the return period increased (Table 8). The LCC lower bound was lowest at P = 2 years, while the upper bound reached its maximum at P = 50 years. The front was steep at low costs and flattened at high costs, reflecting diminishing marginal improvements. The number of front points ranged from 46 to 63, providing adequate coverage, a stable distribution, and sufficient diversity for the subsequent selection and evaluation of representative schemes.

Table 8. Summary of Pareto solutions for different rainfall scenarios.

Return Period (P)	LCC Min (CNY Billion)	LCC Max (CNY Billion)	R_f Min	R_f Max	Number of Frontier Points
P = 2	2.17	6.43	0.672	0.983	46
P = 5	2.98	6.32	0.692	0.943	63
P = 10	2.94	6.98	0.642	0.922	63
P = 20	3.05	6.51	0.608	0.887	60
P = 50	2.98	7.12	0.545	0.861	58

The dynamics of the multi-objective optimization under each rainfall scenario were examined. Overall, mean LCC declined and mean UDS resilience rose monotonically during iterations, with marginal intergenerational gains diminishing over time. Each optimization group showed a clear inflection point (Table 9), after which changes in LCC and UDS resilience were less than 0.1%. For example, the initial generation mean LCC was about CNY 5.8 billion, dropping to about CNY 3.2 billion in the final generation, a reduction

of roughly CNY 2.6 billion. The initial and final means of UDS resilience decreased as the return period increased. For P = 2, 5, 10, 20, and 50 years, the minimum UDS resilience values were 0.830, 0.760, 0.714, 0.674, and 0.629, while the maximum values were 0.961, 0.923, 0.899, 0.873, and 0.844.

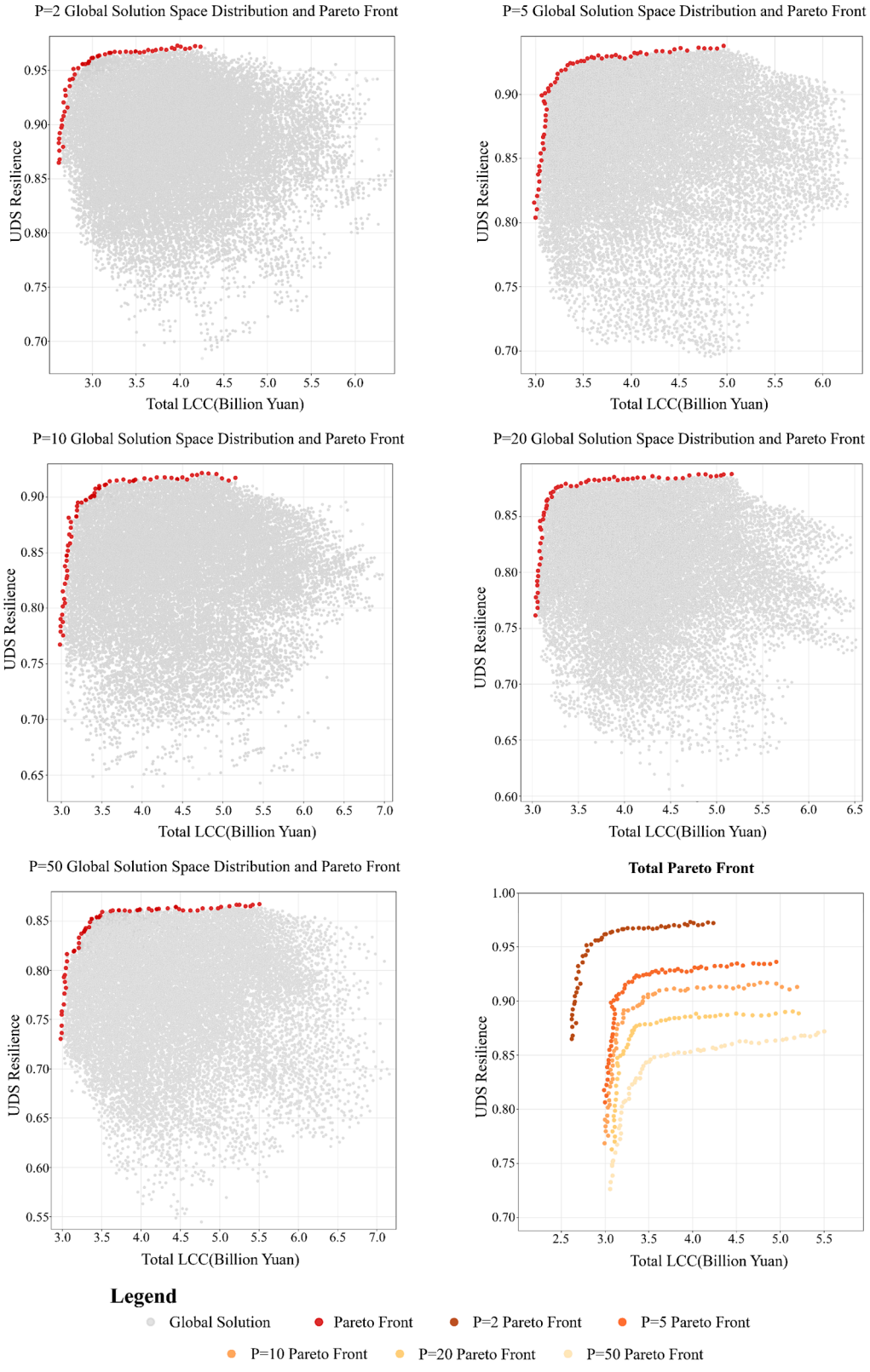


Figure 5. Global solutions and Pareto front for different rainfall scenarios.

Table 9. Multi-objective optimization process summary.

Rainfall Return Period (P)	Initial-Generation Mean LCC (CNY Billion)	Final-Generation Mean LCC (CNY Billion)	Initial-Generation Mean R_f	Final-Generation Mean R_f	Inflection Generation (LCC Mean)	Inflection Generation (R_f Mean)
P = 2	5.804	3.285	0.830	0.961	94	88
P = 5	5.805	3.250	0.760	0.923	92	87
P = 10	5.802	3.151	0.714	0.899	92	90
P = 20	5.800	3.240	0.674	0.873	95	89
P = 50	5.799	3.265	0.629	0.844	94	86

3.4. Comprehensive Evaluation of the Pareto Set

The entropy weights for LCC and UDS resilience were computed for return periods of P = 2, 5, 10, 20, and 50 years (Table 10). As the return period increased, LCC weights rose to 0.71 at P = 20 before falling slightly to 0.69 at P = 50. UDS resilience peaked at P = 5 and stabilized at 0.29–0.31 for P $\geq$ 20.

Table 10. Weights for optimization objectives in TOPSIS process based on the EWM.

Rainfall Return Period (P)	P = 2	P = 5	P = 10	P = 20	P = 50
LCC	0.67	0.61	0.64	0.71	0.69
UDS resilience	0.33	0.39	0.36	0.29	0.31

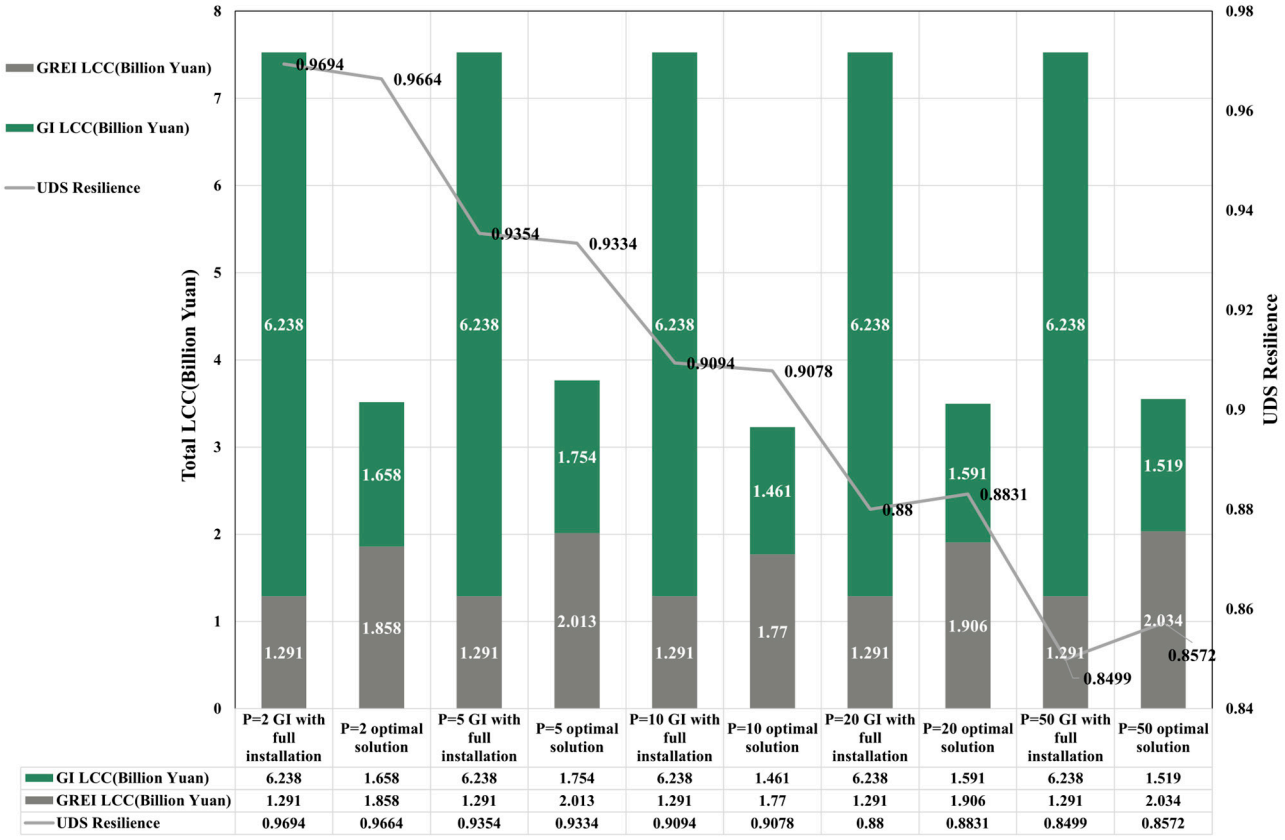
The Pareto fronts for the five return periods were evaluated and ranked using TOPSIS. LCC was treated as a cost-type indicator and UDS resilience as a benefit-type indicator. Data were normalized to the 0–1 interval and multiplied by scenario-specific weights to form the weighted normalized matrix. Positive and negative ideal solutions were then identified, and closeness values were calculated. For each scenario, Table 11 reports the objective values and closeness of the scheme with the highest TOPSIS score. For comparison, the total cost and cost structure of the schemes are summarized as follows. GI cost shares were 47.2%, 46.6%, 45.2%, 45.5%, and 42.8%. In the optimal schemes, UDS resilience decreased steadily with higher return periods, while total LCC ranged from CNY 3.231 to 3.767 billion. This indicates that strong rainfall scenarios required higher costs to achieve resilience, while the attainable resilience upper bound declined. Optimal closeness values (C_i) ranged from 0.7012 to 0.8052, showing that the selected solutions in each scenario were close to the positive ideal solution. The P = 20 years scenario achieved the highest C_i of 0.8052.

Table 11. Final optimal solutions based on TOPSIS for different rainfall scenarios.

Rainfall Return Period (P)	P = 2	P = 5	P = 10	P = 20	P = 50
GREI LCC (CNY billion)	1.858	2.013	1.770	1.906	2.034
GI LCC (CNY billion)	1.658	1.754	1.461	1.591	1.519
UDS-R	0.9664	0.9334	0.9078	0.8831	0.8572
Closeness (C_i)	0.7012	0.7934	0.7715	0.8052	0.7755

As shown in Figure 6, the TOPSIS-optimal schemes were compared with the GI with full installation, defined as installing GI in the maximum suitable area. In the full installation case, the LCC of GI was CNY 6.238 billion, the LCC of GREI was CNY 1.291 billion, and the UDS resilience declined from 0.9694 to 0.8499 as the rainfall return period increased. The total LCC of the optimal schemes decreased by CNY 3.762–4.298 billion across scenarios, averaging a 53.36% reduction. UDS resilience declined slightly at P = 2, 5, and 10 (-0.0030, -0.0020, -0.0016), but increased at P = 20 and 50 (+0.0031, +0.0073). Per CNY 1 billion yuan, resilience changes ranged from -0.0007 to -0.0004 at the lower return period and

from +0.0008 to +0.0018 at the higher return period. The cost composition also shifted considerably. In the full-capacity case, GI accounted for 82.9% and GREI for 17.1%, whereas in the optimal schemes GI dropped to 42.8–47.2% (a reduction of CNY 4.484–4.777 billion, or 71.9–76.6%) and GREI rose to 52.8–57.2% (an increase of CNY 0.479–0.743 billion, or 37.1–57.6%). This reflects a major redistribution of costs between GI and GREI.



	P=2 GI with full installation	P=2 optimal solution	P=5 GI with full installation	P=5 optimal solution	P=10 GI with full installation	P=10 optimal solution	P=20 GI with full installation	P=20 optimal solution	P=50 GI with full installation	P=50 optimal solution
GI LCC(Billion Yuan)	6.238	1.658	6.238	1.754	6.238	1.461	6.238	1.591	6.238	1.519
GREI LCC(Billion Yuan)	1.291	1.858	1.291	2.013	1.291	1.77	1.291	1.906	1.291	2.034
UDS Resilience	0.9694	0.9664	0.9354	0.9334	0.9094	0.9078	0.88	0.8831	0.8499	0.8572

Figure 6. Comparison between the optimal solutions identified by TOPSIS and the GI with full installation (maximum suitable area).

The optimal overlaying pipe networks and GI distribution are presented in Figure 7. It shows the spatial allocation of GI installation in the optimal solutions, with local enlarged views showing detailed diameter changes in the pipe network. Across all scenarios, interventions consistently prioritized the main trunk, were concentrated upstream, and reinforced confluence nodes. As the return period increased, the extent of GREI reinforcement expanded progressively; for example, for P = 2–5 years, upsizing was limited to key backbone segments, whereas for P = 10–50 years, it extended along confluence axes and connectors, forming continuous bands integrated with clustered GI. Overall, higher return periods required greater continuity and redundancy, reflected in stronger banded upsizing. Common characteristics across all scenarios included pipe diameter adjustments concentrated on high-importance segments spatially coupled with nearby GI and the formation of new GI patches as dense clusters or short hydraulic links with upsized pipes. In contrast, GI coverage decreased sharply in peripheral areas with low hydrological contribution.

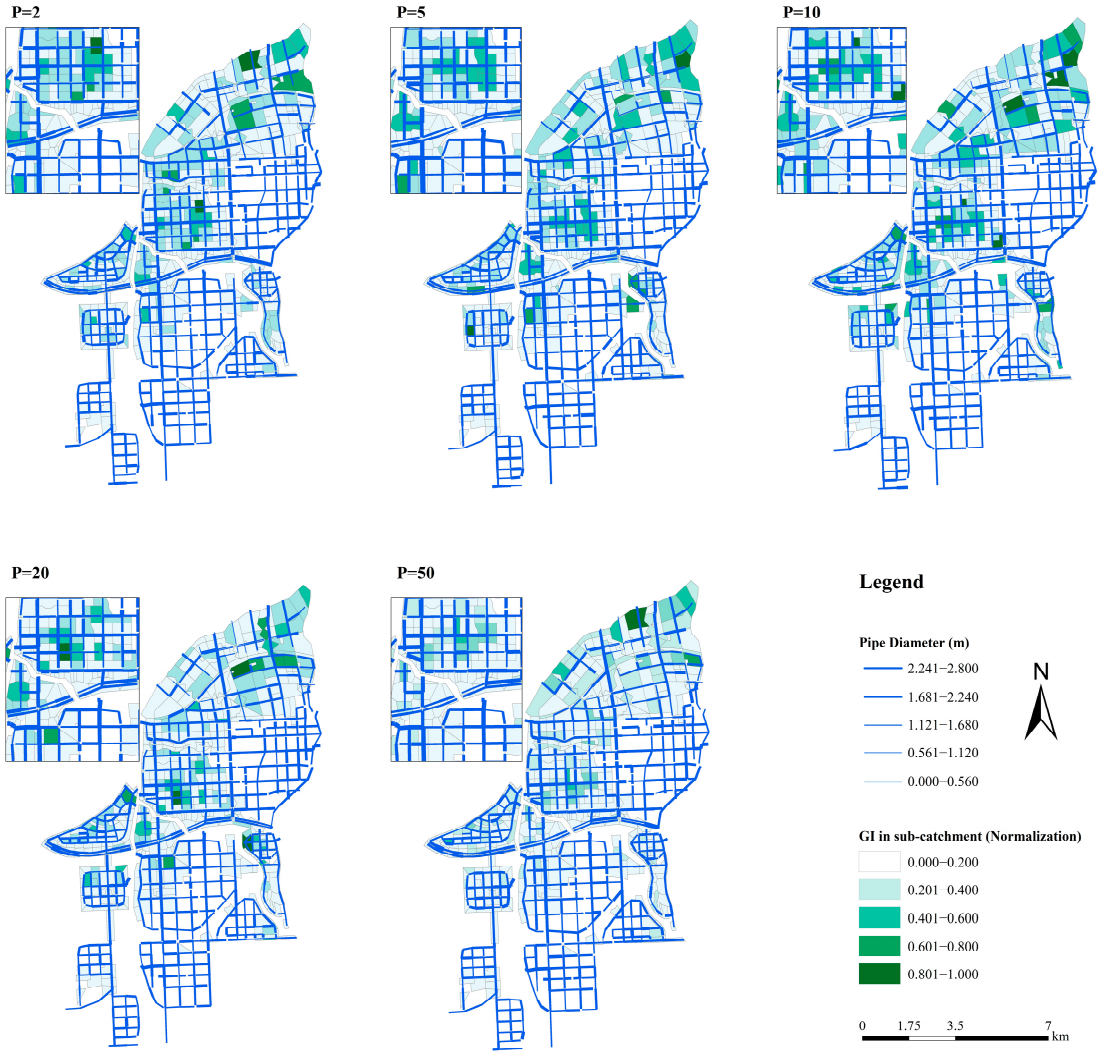


Figure 7. Coupled GI–GREI layouts for different rainfall scenarios.

4. Discussion

4.1. GI Suitability and Drainage Pipe Network Importance Analysis

The high-suitability areas for the three types of GI were concentrated in the northwest, reflecting biophysical and built-environment conditions such as higher roof load capacity, more permeable soils, and gentler slopes. In contrast, the southeast was constrained by weaker buildings and extensive transportation-related impervious surfaces [35,49]. These spatial constraints concentrated GI allocation into high-suitability clusters in the northwest and shifted reliance to GREI in low-suitability areas in the southeast. This duality shaped the balance between cost and resilience observed in the Pareto solutions. Using suitability results as installation zones and upper bounds not only directed the optimization toward realistic GI deployment but also enhanced computational efficiency, in line with recent GI–GREI studies [50].

Based on computed pipe network importance, 6.95%, 15.04%, and 78.01% of segments were assigned to high, medium, and low importance, respectively. On average, high-tier segments were 2.34 times more important than medium-tier segments and 16.02 times more important than low-tier segments. Cumulative importance accounted for roughly 38%, 35%, and 27% of the drainage network across the three tiers. These results revealed a highly uneven distribution of risk. A small fraction of trunk pipelines concentrated much of the system's criticality, whereas peripheral lines, though more numerous, contributed

relatively little. These findings are consistent with related studies that computed network importance and criticality for urban water supply, drainage, and transportation networks, where risk was also unevenly distributed and largely shaped by structural position and connectivity [51]. This spatial heterogeneity underscores the importance of prioritizing reinforcement of high-importance segments, ensuring that GREI interventions are targeted where they deliver the greatest resilience gains.

Spatially, high-value segments were clustered along backbone corridors, reflecting their role in draining large contributing areas and carrying peak flows. Their limited redundancy made them essential for maintaining overall system performance, as failures along these lines could disrupt extensive service areas and cause upstream surcharge. Isolated high-value segments also appeared at confluence nodes, where failure risked local disconnection and reduced drainage accessibility. Similar to earlier observations, downstream drainage segments tended to show higher importance due to flow convergence, with failures producing more severe overflow events [41]. These spatial patterns indicate that reinforcement and monitoring should be directed toward backbone corridors and confluence nodes, linking spatial priorities with system functionality to strengthen resilience. This study advances existing work by incorporating Network Moran's I [52], which statistically verifies spatial clustering along the network. Moving beyond visual interpretation, this method strengthens the reliability of GREI importance patterns and facilitates their transferability to other urban drainage contexts.

4.2. Multi-Objective Optimization

Across the five rainfall scenarios, the Pareto fronts displayed consistent concave shapes. In the low-cost range, modest increases in LCC yielded substantial improvements in UDS resilience, whereas in the high-cost range, the fronts flattened, indicating diminishing returns (Figure 5). The distribution of LCC and UDS resilience showed adequate coverage and dispersion, which highlights the economic–resilience trade-off and indicates that efficient resilience gains can be achieved without maximal investment in GI and GREI [50]. Under light rainfall intensity, GI effectively provides infiltration and retention, offering lower-cost, high-resilience solutions. However, for $P \geq 20$, upstream peak reduction saturates and downstream trunk and confluence capacities become binding constraints, raising LCC and limiting resilience gains. These results underscore the need to optimize GI–GREI allocation with respect to both event magnitude and network capacity, highlighting the priority of reinforcing critical segments under extreme scenarios.

Intergenerational dynamics reveal both algorithm convergence and performance evolution. The mean LCC across scenarios declines from CNY 5.8 to 3.2 billion, while mean UDS resilience steadily increases. Resilience stabilizes earlier (generations 86–90) than LCC (generations 92–95), indicating that the algorithm first secures functional performance before reducing redundant investment. This progression highlights the value of a phased optimization strategy, such as early iterations strengthening system resilience and later ones enhancing economic efficiency, providing practical guidance for cost-effective GI and GREI allocation in urban drainage planning.

The migration of the Pareto front across return periods reflects the interaction between GI performance and system constraints. For $P \leq 10$, GI effectively relieves outfall and trunk pressure through peak reduction, shifting, and flow diversion, producing many low-LCC, high-resilience solutions. For $P \geq 20$, however, GI capacity saturates and downstream bottlenecks dominate, reducing resilience potential and sharply increasing marginal costs. The joint GI–GREI optimization yields significant gains in the low-cost region but smaller incremental benefits thereafter [50,52,53].

4.3. Comprehensive Evaluation by TOPSIS

The entropy weighting results show that LCC consistently holds greater weight than UDS resilience across all scenarios, reflecting its higher information content along the Pareto front. Under extreme rainfall, resilience becomes constrained and solution variability narrows, reducing differences in UDS resilience. Therefore, economic considerations dominate decision-making when system performance nears its physical limits. The Pareto-optimal solutions in each scenario were ranked using TOPSIS. All results are close to their respective ideal solutions. Under moderate-to-high return periods, strategic investment in key GREI segments can substantially enhance the cost–resilience balance, emphasizing the value of targeted optimization over uniform deployment. For example, at P = 20, the Pareto front showed a narrower resilience range, so allocating LCC to reinforce critical trunk or confluence nodes more effectively improved system performance.

Analysis of the objective values and cost structure shows that optimal UDS resilience declines as rainfall return period increases. The total LCC remains relatively stable (CNY 3.231–3.767 billion), indicating that maintaining high resilience requires a consistent baseline investment across scenarios. The GI cost share (42.8–47.2%) suggests that optimal solutions do not rely on maximal GI deployment but leverage the synergy between source infiltration or detention and targeted GREI reinforcement [54]. This aligns with previous studies showing that excessive GI yields diminishing returns [52]. The slight decline in GI share with increasing return period further highlights the importance of coordinating GI–GREI planning under varying hydrological conditions [22,55,56].

Compared with the full-capacity GI situation, the TOPSIS-optimal solutions reduce total LCC when maintaining similar or slightly higher resilience. The key mechanism is cost reallocation. In the full-capacity case, GI accounts for 82.9% of LCC, whereas in the optimal solutions its share drops to 42.8–47.2% and GREI rises to 52.8–57.2%. GI marginal benefits diminish under frequent storms [48], whereas targeted GREI reinforcement at critical trunks and confluence nodes under higher return periods more effectively reduces downstream burden and delivers resilience at lower cost [22].

The five optimal solutions display a consistent spatial pattern featuring backbone prioritization, upstream aggregation, and node reinforcement. Pipe diameter increases form continuous belts along the main axis toward the outfall and primary connector corridors, with minimal adjustments in terminal laterals. GI clusters in large upstream contributing units and along both sides of the backbone, forming dense patches arranged in alternating patch-and-belt patterns. This configuration reflects a coordinated allocation strategy, linking source peak attenuation, main-axis conveyance, and downstream discharge.

This spatial pattern of backbone priority, upstream aggregation, and node reinforcement suggests a coordinated chain of interventions, attenuating peaks at the source, ensuring efficient conveyance along the backbone, and securing discharge capacity downstream. As the return period increases, GREI reinforcement expands along the downstream confluence axis and GI shifts from scattered patches to sheet- and belt-like layouts along the backbone [57]. This suggests that under more stringent scenarios, resilience depends increasingly on continuous conveyance and redundancy, while GI provides peak attenuation and lateral diversion for the trunk system. Compared with the GI with full installation, the optimal solutions shift both GI and GREI from uniform deployment across the study area to a targeted concentration, thereby providing the spatial mechanism by which cost reallocation reduces total LCC while preserving resilience [47].

Recommendations for the Green and Gray Infrastructure Construction Practice

High-suitability parcels, particularly those along main drainage corridors and in large upstream contributing units, should be designated as GI priority belts. In contrast,

areas with low suitability should reduce GI investment to avoid uniform deployment that disperses funds and heightens operation and maintenance burdens.

GREI configuration should be prioritized by integrating pipe network importance into construction decisions. High-importance segments should be added to the priority construction and monitoring list; medium-importance segments should go into long-term plans with scheduled maintenance; low-importance segments should receive routine inspections and minor repairs. Pipe upsizing should form connected chains along outlets and downstream corridors, with synchronous upstream–downstream upgrades, avoiding fragmented spot repairs.

A coupled GI–GREI layout based on multi-objective optimization can balance LCC with urban resilience, strengthening the capacity of cities to withstand climate change. Sponge city planning should therefore integrate multi-objective optimization into GI–GREI construction, with institutionalized review mechanisms to ensure coordination.

4.4. Limitations

This study has several limitations. First, the analysis of GI–GREI effectiveness did not include GREI failure scenarios. Second, due to the large study area and complex pipe-network, the framework did not optimize GREI network topology.

5. Conclusions

This study innovatively incorporated pipe-network importance into a GI–GREI multi-objective optimization framework by coupling PySWMM with NSGA-II, evaluating the Pareto set using entropy-weighted TOPSIS under five rainfall return periods. Across optimization generations, mean LCC decreased by approximately CNY 2.6 billion compared with the initial generation, while UDS resilience improved in all scenarios compared with the initial generation, with the largest gain at P = 50 (+0.215). After TOPSIS evaluation, the optimal schemes reduced total LCC by an average reduction 53.36% compared with the GI full-capacity case. UDS resilience decreased slightly at P = 2, 5, and 10, but increased at P = 20 and 50. The cost composition shifted markedly, with GI decreasing from 82.9% to as low as 47.2% and GREI increasing from 17.1% to as high as 57.2%. These results demonstrate that multi-objective optimization can effectively restructure the composition and spatial allocation of GI–GREI to achieve a more favorable UDS–LCC trade-off and avoid resource misallocation. The proposed framework provides actionable guidance for cost-effective and resilient GI–GREI planning, supporting infrastructure investment decisions and being adaptable to diverse urban contexts for climate-adaptive development.

Future research can progress in two directions. First, projected future rainfall scenarios should be integrated into the GI–GREI multi-objective optimization framework to develop adaptive construction strategies. Second, the optimization of network topology should focus on refining node placement and enhancing pipe connectivity to improve drainage efficiency and cost-effectiveness in complex, large-scale, multilayer, and highly dynamic sewer systems.

Author Contributions: Conceptualization, X.F. and Z.T.; methodology, Z.T. and X.F.; software, Z.T. and Y.L.; validation, Y.M.; formal analysis, Z.T., M.H. and Y.Z.; investigation, Z.T., Y.L. and M.H.; data curation, Z.T., S.H. and Y.M.; writing—original draft preparation, Z.T., Y.L., Y.Z. and Y.M.; writing—review and editing, X.F.; visualization, Z.T., S.H., M.H. and Y.L.; supervision, X.F.; project administration, X.F.; funding acquisition, X.F. and Z.T. All authors have read and agreed to the published version of the manuscript.

Funding: This research was performed and supported while Xin Fu held the funding (2022JM-204) from the Shaanxi Science and Technology Agency, China. Additionally, it received partial funding from the Innovation and Entrepreneurship Training Program for Chinese College Students (S202510712460), led by Z.T.

Data Availability Statement: The data used in this study can be obtained upon request from the corresponding author.

Acknowledgments: We would like to thank Yan Wen and Shanshan Jia for their preliminary review and suggestions. We also appreciate the help of Tongtong Li at Northwest A&F University, who took part in the data collection process.

Conflicts of Interest: The authors declare no conflicts of interest.

References

1. Hathaway, J.M.; Bean, E.Z.; Bernagros, J.T.; Christian, D.P.; Davani, H.; Ebrahimian, A.; Fairbaugh, C.M.; Gulliver, J.S.; McPhillips, L.E.; Palino, G.; et al. A Synthesis of Climate Change Impacts on Stormwater Management Systems: Designing for Resiliency and Future Challenges. *J. Sustain. Water Built Environ.* **2024**, *10*, 04023014. [CrossRef]
2. Zhou, S.; Liu, Z.; Wang, M.; Gan, W.; Zhao, Z.; Wu, Z. Impacts of Building Configurations on Urban Stormwater Management at a Block Scale Using XGBoost. *Sustain. Cities Soc.* **2022**, *87*, 104235. [CrossRef]
3. Jiang, Y.; Li, J.; Li, Y.; Gao, J.; Xia, J. Influence of Rainfall Pattern and Infiltration Capacity on the Spatial and Temporal Inundation Characteristics of Urban Waterlogging. *Environ. Sci. Pollut. Res.* **2024**, *31*, 12387–12405. [CrossRef]
4. Yuan, F.; Xu, Y.; Li, Q.; Mostafavi, A. Spatio-Temporal Graph Convolutional Networks for Road Network Inundation Status Prediction during Urban Flooding. *Comput. Environ. Urban Syst.* **2022**, *97*, 101870. [CrossRef]
5. Zhou, S.; Zhang, D.; Wang, M.; Liu, Z.; Gan, W.; Zhao, Z.; Xue, S.; Müller, B.; Zhou, M.; Ni, X. Risk-Driven Composition Decoupling Analysis for Urban Flooding Prediction in High-Density Urban Areas Using Bayesian-Optimized LightGBM. *J. Clean. Prod.* **2024**, *457*, 142286. [CrossRef]
6. Nika, C.E.; Gusmaroli, L.; Ghafourian, M.; Atanasova, N.; Buttiglieri, G.; Katsou, E. Nature-Based Solutions as Enablers of Circularity in Water Systems: A Review on Assessment Methodologies, Tools and Indicators. *Water Res.* **2020**, *183*, 115988. [CrossRef]
7. Wang, J.; Liu, G.; Wang, J.; Xu, X.; Shao, Y.; Zhang, Q.; Liu, Y.; Qi, L.; Wang, H. Current Status, Existent Problems, and Coping Strategy of Urban Drainage Pipeline Network in China. *Environ. Sci. Pollut. Res.* **2021**, *28*, 43035–43049. [CrossRef] [PubMed]
8. Wang, J.; Liu, J.; Mei, C.; Wang, H.; Lu, J. A Multi-Objective Optimization Model for Synergistic Effect Analysis of Integrated Green-Gray-Blue Drainage System in Urban Inundation Control. *J. Hydrol.* **2022**, *609*, 127725. [CrossRef]
9. Wang, Z.; Zhou, S.; Wang, M.; Zhang, D. Cost-Benefit Analysis of Low-Impact Development at Hectare Scale for Urban Stormwater Source Control in Response to Anticipated Climatic Change. *J. Environ. Manag.* **2020**, *264*, 110483. [CrossRef]
10. Coletta, V.R.; Pagano, A.; Zimmermann, N.; Davies, M.; Butler, A.; Fratino, U.; Giordano, R.; Pluchinotta, I. Socio-Hydrological Modelling Using Participatory System Dynamics Modelling for Enhancing Urban Flood Resilience through Blue-Green Infrastructure. *J. Hydrol.* **2024**, *636*, 131248. [CrossRef] [PubMed]
11. Ambily, P.; Chithra, N.R.; Mohammed Firoz, C. A Framework for Urban Pluvial Flood Resilient Spatial Planning through Blue-Green Infrastructure. *Int. J. Disaster Risk Reduct.* **2024**, *103*, 104342. [CrossRef]
12. Yin, D.; Zhang, X.; Cheng, Y.; Jia, H.; Jia, Q.; Yang, Y. Can Flood Resilience of Green-Grey-Blue System Cope with Future Uncertainty? *Water Res.* **2023**, *242*, 120315. [CrossRef]
13. McFarland, A.R.; Larsen, L.; Yeshitela, K.; Engida, A.N.; Love, N.G. Guide for Using Green Infrastructure in Urban Environments for Stormwater Management. *Environ. Sci. Water Res. Technol.* **2019**, *5*, 643–659. [CrossRef]
14. Ying, J.; Zhang, X.; Zhang, Y.; Bilan, S. Green Infrastructure: Systematic Literature Review. *Econ. Res.-Ekon. Istraživanja* **2022**, *35*, 343–366. [CrossRef]
15. Yang, B.; Zhang, T.; Li, J.; Feng, P.; Miao, Y. Optimal Designs of LID Based on LID Experiments and SWMM for a Small-Scale Community in Tianjin, North China. *J. Environ. Manag.* **2023**, *334*, 117442. [CrossRef]
16. Wang, M.; Chen, F.; Zhang, D.; Chen, Z.; Su, J.; Zhou, S.; Li, J.; Chen, J.; Li, J.; Tan, S.K. Data-Driven Approach to Spatiotemporal Dynamic Risk Assessment of Urban Flooding Based on Shared Socio-Economic Pathways. *Ecol. Indic.* **2023**, *154*, 110764. [CrossRef]
17. Xu, C.; Tang, T.; Jia, H.; Xu, M.; Xu, T.; Liu, Z.; Long, Y.; Zhang, R. Benefits of Coupled Green and Grey Infrastructure Systems: Evidence Based on Analytic Hierarchy Process and Life Cycle Costing. *Resour. Conserv. Recycl.* **2019**, *151*, 104478. [CrossRef]
18. Lu, P.; Sun, Y.; Steffen, N. Scenario-Based Performance Assessment of Green-Grey-Blue Infrastructure for Flood-Resilient Spatial Solution: A Case Study of Pazhou, Guangzhou, Greater Bay Area. *Landsc. Urban Plan.* **2023**, *238*, 104804. [CrossRef]

19. Kim, J.; Kang, J. Development of Hazard Capacity Factor Design Model for Net-Zero: Evaluation of the Flood Adaptation Effects Considering Green-Gray Infrastructure Interaction. *Sustain. Cities Soc.* **2023**, *96*, 104625. [CrossRef]
20. Liu, Z.; Han, Z.; Shi, X.; Liao, X.; Leng, L.; Jia, H. Multi-Objective Optimization Methodology for Green-Gray Coupled Runoff Control Infrastructure Adapting Spatial Heterogeneity of Natural Endowment and Urban Development. *Water Res.* **2023**, *233*, 119759. [CrossRef] [PubMed]
21. Liu, M.; Lai, C.; Zhang, Y.; Chen, B.; Wang, M. Multi-Objective Optimisation of Integrated Grey-Green Infrastructure in Response to Climate Change from a Life Cycle Perspective. *J. Clean. Prod.* **2025**, *498*, 145162. [CrossRef]
22. Tansar, H.; Duan, H.-F.; Mark, O. A Multi-Objective Decision-Making Framework for Implementing Green-Grey Infrastructures to Enhance Urban Drainage System Resilience. *J. Hydrol.* **2023**, *620*, 129381. [CrossRef]
23. Vörösmarty, C.J.; Stewart-Koster, B.; Green, P.A.; Boone, E.L.; Flörke, M.; Fischer, G.; Wiberg, D.A.; Bunn, S.E.; Bhaduri, A.; McIntyre, P.B. A Green-Gray Path to Global Water Security and Sustainable Infrastructure. *Glob. Environ. Change* **2021**, *70*, 102344. [CrossRef]
24. Mao, Y.; Li, Y.; Bai, X.; Yang, X.; Han, Y.; Fu, X. Scenario-Based Green Infrastructure Installations for Building Urban Stormwater Resilience—A Case Study of Fengxi New City, China. *Sustainability* **2024**, *16*, 3990. [CrossRef]
25. Zhou, S.; Diao, H.; Wang, J.; Jia, W.; Xu, H.; Xu, X.; Wang, M.; Sun, C.; Qiao, R.; Wu, Z. Multi-Stage Optimization Framework for Synergetic Grey-Green Infrastructure in Response to Long-Term Climate Variability Based on Shared Socio-Economic Pathways. *Water Res.* **2025**, *274*, 123091. [CrossRef]
26. Ye, C.; Gao, J.; Nachabe, M.; Charkhgard, H.; Zhang, Y.; Zhang, Q. Optimization of Green and Grey Infrastructure for Performance Enhancement of Urban Drainage System under Future Conditions. *J. Environ. Manag.* **2025**, *376*, 124518. [CrossRef] [PubMed]
27. Jia, H.; Liu, Z.; Xu, C.; Chen, Z.; Zhang, X.; Xia, J.; Yu, S.L. Adaptive Pressure-Driven Multi-Criteria Spatial Decision-Making for a Targeted Placement of Green and Grey Runoff Control Infrastructures. *Water Res.* **2022**, *212*, 118126. [CrossRef] [PubMed]
28. Zheng, J.; Li, J.; Zeng, J.; Huang, G.; Chen, W. Application of a Time-Dependent Performance-Based Resilience Metric to Establish the Potential of Coupled Green-Grey Infrastructure in Urban Flood Management. *Sustain. Cities Soc.* **2024**, *112*, 105608. [CrossRef]
29. Liu, Z.; Xu, C.; Xu, T.; Jia, H.; Zhang, X.; Chen, Z.; Yin, D. Integrating Socioecological Indexes in Multiobjective Intelligent Optimization of Green-Grey Coupled Infrastructures. *Resour. Conserv. Recycl.* **2021**, *174*, 105801. [CrossRef]
30. Zhang, Y.; Yin, H.; Zhang, D.; Kong, F.; Xu, J.; Wang, M.; Yuan, H. Enhancing Resilience of Green-Grey Infrastructure by Integrating Two Redundancy Strategies into a Multi-Objective Optimization and Service Period Assessment Framework. *Sustain. Cities Soc.* **2025**, *128*, 106474. [CrossRef]
31. Chen, W.; Wang, W.; Mei, C.; Chen, Y.; Zhang, P.; Cong, P. Multi-Objective Decision-Making for Green Infrastructure Planning: Impacts of Rainfall Characteristics and Infrastructure Configuration. *J. Hydrol.* **2024**, *628*, 130572. [CrossRef]
32. Zhou, S.; Jia, W.; Wang, M.; Liu, Z.; Wang, Y.; Wu, Z. Synergistic Assessment of Multi-Scenario Urban Waterlogging through Data-Driven Decoupling Analysis in High-Density Urban Areas: A Case Study in Shenzhen, China. *J. Environ. Manag.* **2024**, *369*, 122330. [CrossRef] [PubMed]
33. Bakhshipour, A.E.; Bakhshizadeh, M.; Dittmer, U.; Haghighi, A.; Nowak, W. Hanging Gardens Algorithm to Generate Decentralized Layouts for the Optimization of Urban Drainage Systems. *J. Water Resour. Plan. Manag.* **2019**, *145*, 04019034. [CrossRef]
34. Zhu, Y.; Xu, C.; Liu, Z.; Yin, D.; Jia, H.; Guan, Y. Spatial Layout Optimization of Green Infrastructure Based on Life-Cycle Multi-Objective Optimization Algorithm and SWMM Model. *Resour. Conserv. Recycl.* **2023**, *191*, 106906. [CrossRef]
35. Guo, K.; Guan, M.; Yu, D. Urban Surface Water Flood Modelling—A Comprehensive Review of Current Models and Future Challenges. *Hydrol. Earth Syst. Sci.* **2021**, *25*, 2843–2860. [CrossRef]
36. Minh Hai, D. Optimal Planning of Low-Impact Development for TSS Control in the Upper Area of the Cau Bay River Basin, Vietnam. *Water* **2020**, *12*, 533. [CrossRef]
37. Zhang, Y.; Wang, M.; Zhang, D.; Lu, Z.; Bakhshipour, A.E.; Liu, M.; Jiang, Z.; Li, J.; Tan, S.K. Multi-Stage Planning of LID-GREI Urban Drainage Systems in Response to Land-Use Changes. *Sci. Total Environ.* **2023**, *859*, 160214. [CrossRef]
38. Dong, X.; Yi, W.; Yuan, P.; Song, Y. Optimization and Trade-off Framework for Coupled Green-Grey Infrastructure Considering Environmental Performance. *J. Environ. Manag.* **2023**, *329*, 117041. [CrossRef]
39. Zhang, X.; Jia, H. Low Impact Development Planning through a Comprehensive Optimization Framework: Current Gaps and Future Perspectives. *Resour. Conserv. Recycl.* **2023**, *190*, 106861. [CrossRef]
40. Zhang, Y.; Yin, H.; Liu, M.; Kong, F.; Xu, J. Evaluating the Effectiveness of Environmental Sustainability Indicators in Optimizing Green-Grey Infrastructure for Sustainable Stormwater Management. *Water Res.* **2025**, *272*, 122932. [CrossRef] [PubMed]
41. Wang, M.; Zhang, Y.; Bakhshipour, A.E.; Liu, M.; Rao, Q.; Lu, Z. Designing Coupled LID–GREI Urban Drainage Systems: Resilience Assessment and Decision-Making Framework. *Sci. Total Environ.* **2022**, *834*, 155267. [CrossRef]
42. Houle, J.J.; Roseen, R.M.; Ballestero, T.P.; Puls, T.A.; Sherrard, J. Comparison of Maintenance Cost, Labor Demands, and System Performance for LID and Conventional Stormwater Management. *J. Environ. Eng.* **2013**, *139*, 932–938. [CrossRef]
43. MortezaNia, S.; Othman, F. Cost Analysis of Pipes for Application in Sewage Systems. *Mater. Des.* **2012**, *33*, 356–361. [CrossRef]

44. Liu, Y.; Zhang, X.; Liu, J.; Wang, Y.; Jia, H.; Tao, S. A Flood Resilience Assessment Method of Green-Grey-Blue Coupled Urban Drainage System Considering Backwater Effects. *Ecol. Indic.* **2025**, *170*, 113032. [CrossRef]
45. Zhang, W.; Wang, W.; Zhang, Y.; Wang, F.; Sun, S. Determining the Optimal Degradation Rate of Biodegradable Films in a Maize Farmland Based on the EWM-TOPSIS Model. *Agric. Water Manag.* **2025**, *309*, 109359. [CrossRef]
46. Ma, H.; Zhang, Y.; Sun, S.; Liu, T.; Shan, Y. A Comprehensive Survey on NSGA-II for Multi-Objective Optimization and Applications. *Artif. Intell. Rev.* **2023**, *56*, 15217–15270. [CrossRef]
47. Liu, Y.; Xiong, Z.; Wang, M.; Zhang, M.; Adnan, R.M.; Fu, W.; Sun, C.; Tan, S.K. Decentralized Coupled Grey–Green Infrastructure for Resilient and Cost-Effective Stormwater Management in a Historic Chinese District. *Water* **2025**, *17*, 2325. [CrossRef]
48. Wang, M.; Liu, M.; Zhang, D.; Qi, J.; Fu, W.; Zhang, Y.; Rao, Q.; Bakhshipour, A.E.; Tan, S.K. Assessing and Optimizing the Hydrological Performance of Grey-Green Infrastructure Systems in Response to Climate Change and Non-Stationary Time Series. *Water Res.* **2023**, *232*, 119720. [CrossRef]
49. Apud, A.; Faggian, R.; Sposito, V.; Martino, D. Suitability Analysis and Planning of Green Infrastructure in Montevideo, Uruguay. *Sustainability* **2020**, *12*, 9683. [CrossRef]
50. Wang, L.; Zhao, J.; Xiong, Z.; Zhuang, J.; Wang, M. Integrating Grey–Green Infrastructure in Urban Stormwater Management: A Multi–Objective Optimization Framework for Enhanced Resilience and Cost Efficiency. *Appl. Sci.* **2025**, *15*, 3852. [CrossRef]
51. Barati, H.; Yazici, A.; Almotahari, A. A Methodology for Ranking of Critical Links in Transportation Networks Based on Criticality Score Distributions. *Reliab. Eng. Syst. Saf.* **2024**, *251*, 110332. [CrossRef]
52. Wang, J.; Liu, J.; Wang, H.; Mei, C. Approaches to Multi-Objective Optimization and Assessment of Green Infrastructure and Their Multi-Functional Effectiveness: A Review. *Water* **2020**, *12*, 2714. [CrossRef]
53. Li, E.; Fu, X.; Song, J.; Jing, L.; Zhang, B.; Wang, X. Developing a Decision Support System for Regulating Urban Runoff by Centralized Blue-Green Infrastructure. *Environ. Impact Assess. Rev.* **2026**, *117*, 108190. [CrossRef]
54. Yao, Y.; Li, J.; Lv, P.; Li, N.; Jiang, C. Optimizing the Layout of Coupled Grey-Green Stormwater Infrastructure with Multi-Objective Oriented Decision Making. *J. Clean. Prod.* **2022**, *367*, 133061. [CrossRef]
55. Wang, M.; Jiang, Z.; Zhang, D.; Zhang, Y.; Liu, M.; Rao, Q.; Li, J.; Keat Tan, S. Optimization of Integrating Life Cycle Cost and Systematic Resilience for Grey-Green Stormwater Infrastructure. *Sustain. Cities Soc.* **2023**, *90*, 104379. [CrossRef]
56. Sun, C.; Rao, Q.; Xiong, Z.; Liu, M.; Liu, Y.; Fan, C.; Li, J.; Keat Tan, S.; Wang, M.; Zhang, D. Optimized Resilience Coupled with Cost-Effectiveness for Grey and Green Infrastructure: A Case Study in a Historical and Cultural Area, Guangzhou, China. *Ecol. Indic.* **2024**, *167*, 112684. [CrossRef]
57. Mulenga, K.; Zhao, X.; Xie, M.; Chikamba, C. Investigating the Root Causes of Major Failures of Critical Components–With a Case Study of Asbestos Cement Pipes. *Eng. Fail. Anal.* **2018**, *84*, 121–130. [CrossRef]

Disclaimer/Publisher's Note: The statements, opinions and data contained in all publications are solely those of the individual author(s) and contributor(s) and not of MDPI and/or the editor(s). MDPI and/or the editor(s) disclaim responsibility for any injury to people or property resulting from any ideas, methods, instructions or products referred to in the content.